Near Surface Geophysics, 2007, 307-317

Geophysical surveying an active well catchment in the presence of significant topography and anthropogenic disturbances

Hendrik Paasche[1,2*], Jens Tronicke[1,2], Hansruedi Maurer[1], Alan G. Green[1], Esben Auken[3] and Fritz Stauffer[4]

[1] *Institute of Geophysics, Swiss Federal Institute of Technology (ETH), ETH-Hoenggerberg, CH-8093 Zurich, Switzerland*
[2] *Now at: Institute of Geosciences, University of Potsdam, P.O. Box 601553, D-14414 Potsdam, Germany*
[3] *HydroGeophysics Group, Department of Earth Sciences, University of Aarhus, Finlandsgade 8, DK-8200 Aarhus N, Denmark*
[4] *Institute of Hydromechanics and Water Management, Swiss Federal Institute of Technology (ETH), ETH-Hoenggerberg, CH-8093 Zurich, Switzerland*

Received October 2005, revision accepted April 2007

ABSTRACT

Traditional approaches to surveying well catchments usually involve investigations at two quite different spatial scales: very high resolution borehole-based studies and low resolution tracer and pump tests. In recent years, various researchers have attempted to fill the wide gap between the two scales of acquired data by using a variety of geophysical tools that have high-to-medium resolution capabilities. Although geophysical surveying may be relatively straightforward at many locations, there are numerous regions where topography, the presence of ubiquitous metal objects and/or a lack of suitably placed boreholes cause the acquisition, processing, inversion and interpretation of certain types of geophysical data to be extremely challenging. It was necessary for us to address such problems in an investigation of an active well catchment near Zurich, Switzerland. The principal goals of our project were to determine the geometries and physical properties of the shallow sedimentary layers, with emphasis on a key water-bearing gravel unit. To achieve these goals, four different geophysical methods were employed. In a first step, frequency-domain electromagnetic measurements allowed the locations of buried metal pipes to be established. A 2D tomographic seismic refraction survey then provided information on the interface between the low-velocity surface loamy topsoil and underlying high-velocity morainal material. The high electrical resistivity of the important gravel unit allowed its upper boundary to be outlined in 2D models derived from geoelectric data and its lower boundary to be delineated in models based on 1D linked inversions of geoelectric and transient electromagnetic data.

INTRODUCTION

Information on the location, size and geometry of unconsolidated sedimentary units that control groundwater storage and flow is an important prerequisite for characterizing active well catchments. Standard approaches to investigating well catchments include analyses of drill cores, water samples and geophysical logs from sparsely distributed boreholes and tracer and/or pump tests. The borehole data provide local one-dimensional (1D) details, whereas tracer and pump tests usually yield aggregate estimates of aquifer properties across an investigation site (Rubin 2003).

Since most unconsolidated sedimentary units are highly heterogeneous and well catchments may extend over many square kilometres, it is generally difficult to correlate features observed in sparsely distributed boreholes. Geophysical data can be used to relate very high resolution borehole information with the results of low resolution tracer and pump tests (Rubin *et al.* 1992). Most geophysical exploration techniques have been employed in catchment-scale hydrogeophysical studies, with geoelectric, electromagnetic and seismic methods being the methods of choice for the majority of investigators (Fitterman and Stewart 1986; Palacky and Stephens 1990; Goldman and Neubauer 1994; Young *et al.* 1997; Osella *et al.* 1999; Shtivelman and Goldman 2000; Edet and Okereke 2002; Danielsen *et al.* 2003; Gabriel *et al.* 2003; Jørgensen *et al.* 2003; Rubin and Hubbard 2005).

* hendrik@geo.uni-potsdam.de

© 2007 European Association of Geoscientists & Engineers

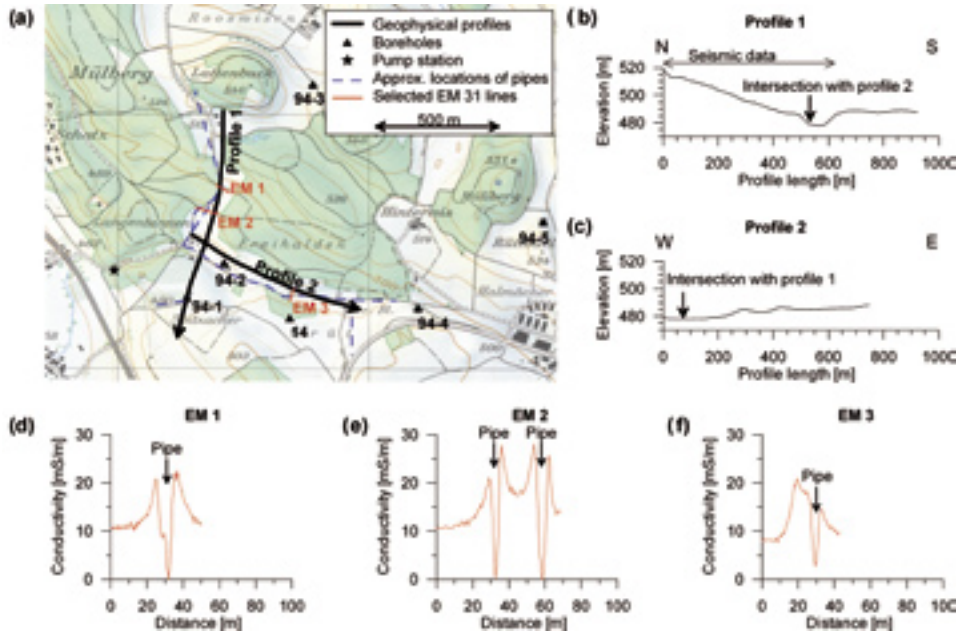

FIGURE 1
(a) Part of the 1:25 000 Swiss topographic map covering the Baltenswil well catchment showing the locations of boreholes, buried pipes and profiles along which various geophysical data were acquired. (b) and (c) Surface topography of geophysical profiles 1 and 2. Seismic data were only collected along the first ~623 m of profile 1. (d)–(f) Selected EM 31 data showing the locations of buried pipes.

At numerous locations, results of single-technique studies may be highly ambiguous (Vozoff and Jupp 1975; Raiche *et al.* 1985). To obtain reliable subsurface knowledge in such regions, combined analyses of several types of geophysical data may be required. This can be achieved either qualitatively (Shtivelman and Goldmann 2000; Gabriel *et al.* 2003; Jørgensen *et al.* 2003) or quantitatively via joint inversions (Raiche *et al.* 1985; Sandberg 1993; Maier *et al.* 1995; Auken *et al.* 2001).

Under favourable conditions, the acquisition, processing, inversion and interpretation of surface-based geophysical data can be relatively straightforward, but in many environments these same actions can be very challenging. The following issues that affect geophysical investigations at our target catchment in northern Switzerland (Fig. 1) are common worldwide:

- undulating topography,
- buried metal pipes and other metal objects,
- lack of sufficient boreholes,
- limited accessibility,
- restrictive groundwater protection policies (e.g. dynamite for seismic surveying and existing boreholes or direct push technologies for logging purposes are forbidden).

In this contribution, we show how an integrated interpretation of selected geophysical data can provide useful information on the target catchment area. We employ the frequency-domain electromagnetic, tomographic seismic refraction, transient electromagnetic (TEM) and geoelectric methods. Individual analyses of the different data sets and linked inversions of the geoelectric and transient electromagnetic measurements along two profiles provide the physical property models on which the integrated interpretation is based.

After describing the target catchment area, we present in some detail the results of our geophysical investigations along one of the profiles. This is followed by a relatively brief discussion of the key results obtained along the second profile. Finally, we outline a strategy for exploring the entire catchment area.

THE BALTENSWIL WELL CATCHMENT

Site description

The Baltenswil protected well catchment (Amt für Abfall, Wasser, Energie und Luft Kanton Zurich 1998; Onnis *et al.* 2004, 2005) underlies a hilly landscape in northern Switzerland, approximately 10 km north-east of Zurich. Figure 1(a) provides an overview of the ~1–2 km^2 investigation site. The surface topography varies from 460 to 550 m (above sea-level). Approximately half of the site is densely forested and the other half is used for intensive farming. Located close to an industrialized urban area, there are heavily used railway lines, powerlines, roads and buried pipes that either transect or lie close to the site. Six boreholes are used to monitor the groundwater level and quality and a pumping station is situated near the south-west corner of the site.

Geophysical data were recorded along two corridors (Fig. 1a). We employed an EM 31 (McNeill 1980) ground-conductivity instrument to map the locations of buried metal pipes within these corridors. Typical EM 31 data are presented in Fig. 1(d–f) and our estimates of the pipe locations are shown in Fig. 1(a). Acquisition of other geophysical data was concentrated along profiles 1 and 2. The elevation changes by ~40 m along profile 1, with some parts of the profile being quite steep (Fig. 1b). By com parison, the elevation varies by only ~10 m along profile 2 (Fig. 1c).

Geology and hydrogeology

Lithologies encountered in the six boreholes can be described in terms of four principal layers (Fig. 2). An upper 1–6 m thick layer of heterogeneous loamy topsoil is underlain by a variably

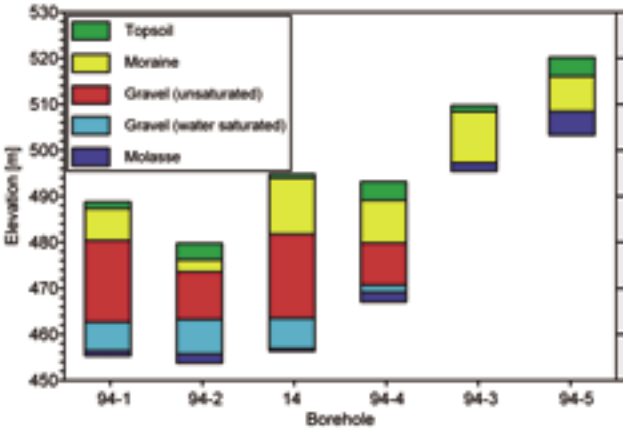

FIGURE 2
Lithological information determined from the six boreholes (see Fig. 1). The gravel layer detected in boreholes 94-1, 94-2, 14 and 94-4 is the aquifer used for regional water supplies. It is not detected in boreholes 94-3 and 94-5.

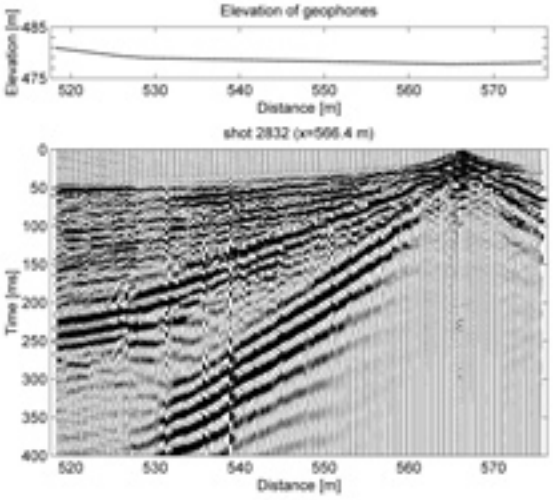

FIGURE 3
Typical seismic shot gather 2832 recorded along profile 1. Surface topography is shown above the gather.

thick morainal layer of sand, silt, gravel and loam. In four of the boreholes, a gravel layer underlies the moraine. This gravel layer is of particular interest for this study because its lower water-saturated part is the shallow aquifer from which water is extracted. No distinct gravel layer and, therefore, no evidence for a shallow aquifer is observed in the northern and eastern boreholes 94-3 and 94-5. In all boreholes, the deepest unit is a weathered layer of Molasse sedimentary rock that acts as an aquitard.

DATA ACQUISITION, PROCESSING AND INVERSION RESULTS

Seismic survey: profile 1

Data acquisition and processing

To obtain estimates of P-wave velocity in the shallow subsurface at the Baltenswil investigation site, seismic data were recorded along an ~623 m length of profile 1 (see Fig. 1b) using six linked 24-channel Geometrics Geode systems with 30 Hz geophones spaced at 0.4 m intervals. The temporal sampling interval was 0.125 ms. A pipegun seismic source with blank cartridges placed ~0.5 m below the surface generated energy at 3.2 m intervals along the length of the seismic line. A typical shot gather is shown in Fig. 3.

First arrivals were picked semi-automatically using a neural-network picking tool implemented in the ProMAX software package (Landmark Graphics Corporation, Houston, Texas). To compensate for interference of first arrivals with source-generated noise and low signal-to-noise ratios at longer offsets, numerous interventions in the picki ng process were required. The maximum distances at which first arrivals could be picked reliably was ~100 m. Picking accuracy varied from ~1 ms for short source–receiver offsets to ~2 ms for longer offsets. In total, more than 34 000 picked traveltimes were considered for inversion.

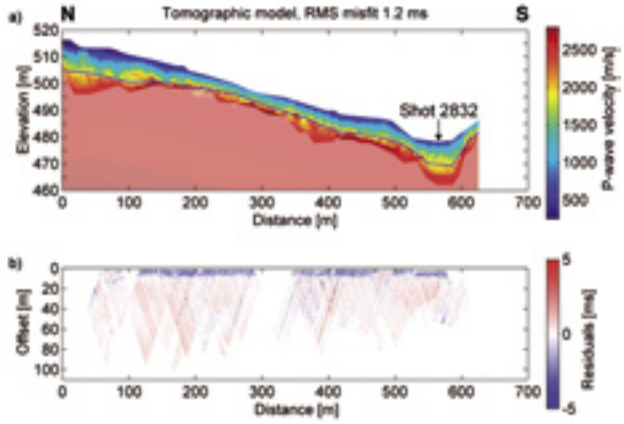

FIGURE 4
(a) Seismic velocity model based on a tomographic inversion of first-arrival traveltime picks. The strong velocity gradient in the very shallow subsurface prevents rays from penetrating to depths greater than 10–20 m (regions covered by the semi-transparent screen are not sampled by rays in the final model). The solid line outlines the picked transition from relatively low to relatively high P-wave velocities. (b) Differences between traveltimes computed for the model shown in (a) and the observed traveltimes.

Seismic refraction tomography

Our seismic refraction tomographic inversion algorithm was based on a finite-difference solution of the eikonal equation (Lanz *et al.* 1998). The model space was represented by a grid of 0.2 × 0.2 m cells. After 12 iterations of the regularized least-squares inversion scheme that was controlled 20% by the damping, 40% by the smoothing and 40% by the data (equation (6) in Lanz *et al.* 1998), the velocity model shown in Fig. 4 was obtained. The root-mean-square (RMS) difference between the

observed traveltimes and those predicted by the final model was 1.2 ms (see also Fig. 4b), comparable to the 1–2 ms picking accuracy.

The P-wave velocities in the final model (Fig. 4) increase abruptly from <330 m/s near the surface to >2000 m/s at shallow depths of only ~5–10 m. Such a velocity contrast can be explained by a sharp transition from damp loamy topsoil (P-wave velocity 200–1200 m/s; Fertig 1997) to moraine (1500–2700 m/s), but not by a transition to dry gravel (180–550 m/s). Accordingly, we interpret the abrupt velocity contrast as the boundary between the loamy topsoil and the underlying morainal material.

2D geoelectric survey: profile 1

Data acquisition and processing

Our 2D geoelectric data were recorded using a GeoTom multi-electrode system (Geolog2000, Augsburg, Germany). To measure very low voltages down to ~100 μV (as was required for recording some of the long-offset dipole–dipole data), this system used a lock-in amplifier to suppress contributions to the recorded signal at frequencies other than the input current frequency of 8.33 Hz. Prior to data acquisition, the ground coupling of each electrode was tested. This was achieved via a series of two-pole measurements between adjacent electrodes using the maximum 50 mA current. Contact resistivities varied from 0.5 to 3.5 kΩ, indicating generally good electrode coupling. To determine each apparent resistivity value, two independent voltage measurements based on the amplitudes of four consecutive cycles of consistently good-quality data were stacked.

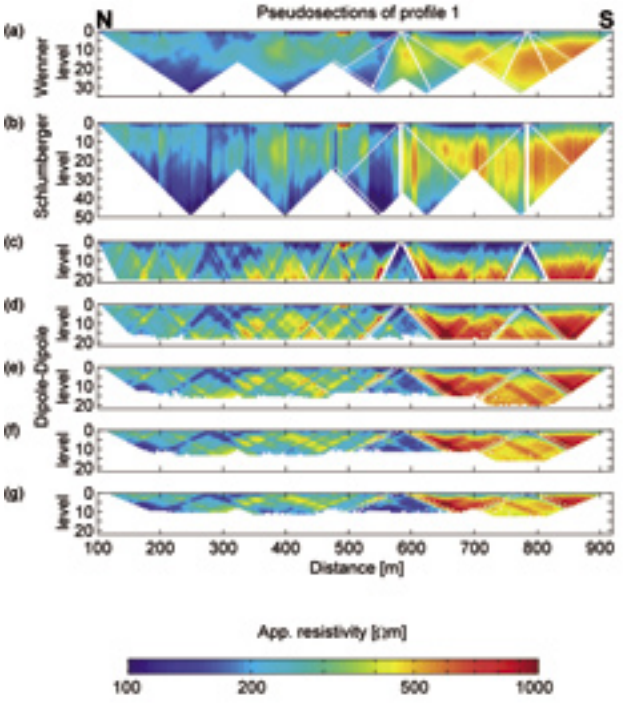

FIGURE 5

Pseudosections determined from geoelectric resistivity data acquired along profile 1 using (a) Wenner (33 data levels), (b) Schlumberger (48 data levels) and (c) –(g) dipole–dipole (dipole lengths of 3, 6, 9, 12 and 15 m provided 20, 18, 20, 16 and 12 useful data levels, respectively) configurations. Minimum electrode spacing for all configurations was 3 m. Data not recorded because of local logistical problems are identified by white dots or lines.

We used a roll-along technique and standard Wenner, Schlumberger and dipole–dipole electrode configurations to record the 2D geoelectric data (Dahlin 2001). For each segment, 100 stainless-steel electrodes were deployed at 3 m intervals (i.e. a total length of 297 m per recording segment). The electrode spread was rolled along the profile by moving 25 or 50 electrodes from the beginning to the end of a segment. The segments overlapped by at least 50 electrodes. Complete Wenner and Schlumberger (potential electrodes separated by 3 m) data sets were recorded along the length of each segment. Using dipole lengths of 3, 6, 9, 12 and 15 m, we recorded 17–20 pseudosection levels of data per dipole–dipole length. Continuous inspections of the pseudosections in real time, and repeat measurements wherever necessary, resulted in generally high signal-to-noise data. Nevertheless, some of the long-offset dipole–dipole data were of sufficiently low quality that they were not included in the inversion process.

The seven pseudosections of electrical resistivity data recorded along profile 1 are shown in Fig. 5. After the final quality control, more than 31 000 data points were included in the inversion process.

Results of 2D tomographic inversions

To invert our various geoelectric data sets, we employ a modified version of the Res2Dinv software (Loke and Barker 1996), which uses inverse Schwartz–Christoffel grid distortion to account for the effects of surface topography (Loke 2000). All data subsets are inverted using the L_2-norm (i.e. least-squares) option and identical regularization parameters (initial damping and minimum damping are 0.2 and 0.03, respectively, and the horizontal cell dimension is set equal to the 3 m electrode spacing). Figure 6 shows the electrical resistivity models that result from tomographically inverting the individual Wenner, Schlumberger, dipole–dipole and combined data sets. Regions of the models covered by transparent screens are distorted by artefacts caused by buried metal pipes and the metal casing of borehole 94-1 (see also Fig. 1a). As a measure of the misfit between the recorded data (either geoelectric or TEM) and resistivities predicted by a model, we use the RMS difference normalized by the average variance of the data (see equation (27) in Auken and Christiansen 2004). Normalized RMS misfits of less than 1 indicate high correspondence, whereas values approaching 2 or more indicate low correspondence. For the Wenner, Schlumberger, dipole–dipole and combined models of Fig. 6, the RMS misfits normalized to a base error of 3% are 0.6, 1.1, 1.5 and 1.3, respectively. Detailed analysis demonstrates that the largest differences

between the recorded data and model predictions occur in regions disturbed by the metal pipes and borehole casing; the three-dimensional (3D) nature of such structures is not included in the inversion process.

All four models in Fig. 6 are distinguished by quasi-layered structures. Based on information extracted from the boreholes (Fig. 2), the intermediate resistivities (several 100 Ωm) in the upper ~8 m of the models represent the topsoil and morainal layers, whereas the underlying highly resistive (>600 Ωm) zone, the thickness and resistivity of which increases in a southerly direction, mostly corresponds to the gravel layer. Although the resistivity of the groundwater ranges from only 13 to 14 Ωm (A. Onnis 2005, pers. comm.), the boundary between unsaturated and saturated parts of the gravel layer is not resolved in any of the geoelectric models. At the base of the models, the intermediate-to-low (~100 Ωm and less) resistivities appear to be associated with the weathered Molasse sedimentary rocks.

The boundaries of the highly resistive zone probably delineate the upper and lower limits of the Baltenswil aquifer. At the upper boundary, all four models contain a relatively sharp transition from the intermediate resistivities of the morainal material to the higher resistivities of the gravel. In contrast, the character of the lower boundary between the gravel and weathered Molasse sedimentary rocks appears to be much more gradational in the dipole–dipole model (Fig. 6c) than the others (Fig. 6a,b,d). This difference simply represents the relatively low sensitivity of the dipole–dipole electrode configuration to vertical variations in resistivity (Dahlin and Zhou 2004). According to theoretical and experimental studies (Stummer *et al*. 2004), models that result from inverting combinations of data recorded with different standard electrode configurations should contain more information over a greater depth range than models determined from the individual data sets. Since the combined model of Fig. 6(d) seems to confirm this expectation, it is the basis for our interpretation. Figure 7 demonstrates that the pseudosections predicted by this model match well the pseudosections derived from the recorded data in Fig. 5.

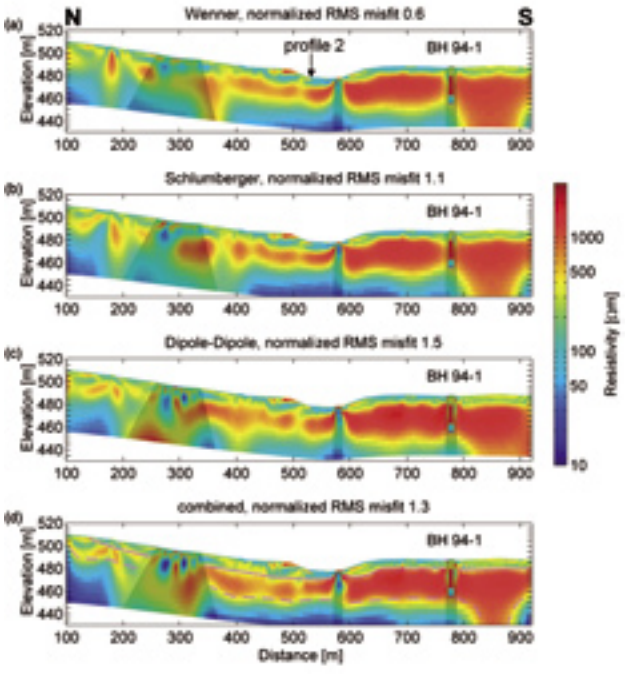

FIGURE 6

2D resistivity models for profile 1 obtained by inverting the (a) Wenner, (b) Schlumberger, (c) dipole–dipole and (d) combined data sets. The influence of topography was included in the inversions. Transparent screens delineate regions disturbed by the effects of buried metal pipes and the metal casing of borehole 94-1. Solid and dashed purple lines in (d) delineate the picked upper and lower boundaries of the highly resistive zone, respectively. Lithologies in borehole 94-1 are described in Fig. 2. The nomalized RMS misfits of 0.6, 1.1, 1.5 and 1.3 shown at the top of the sections correspond to conventional RMS misfits of 1.8%, 3.0%, 8.5% and 8.4%, respectively.

Transient electromagnetic (TEM) survey: profile 1

Data acquisition and processing

We used a ProTEM 47D with a single-turn 10 × 10 m transmitter loop and a ten-turn 1 m radius receiver loop to collect our TEM data. An offset configuration with 25 m spacing between the loop centres and a station spacing of 10 m was employed. After

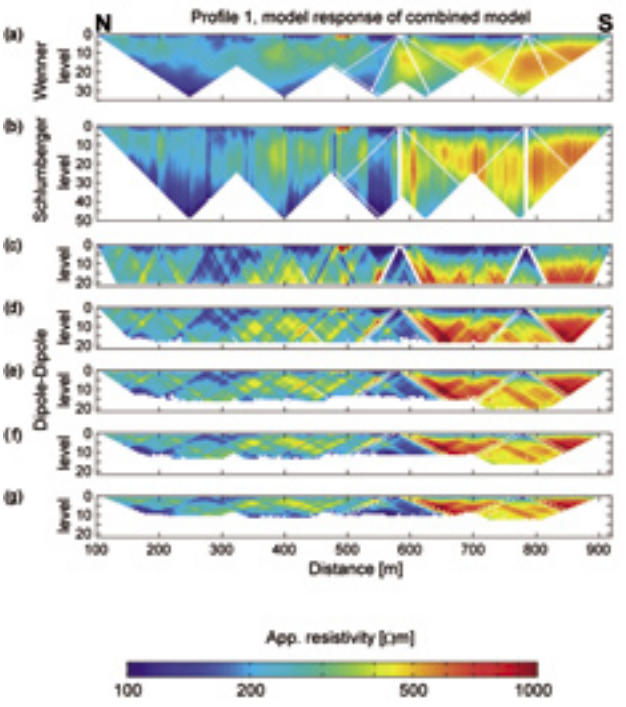

FIGURE 7

Computed pseudosections for the combined model shown in Fig. 6. Comparison with Fig. 5 demonstrates the good fit between observed and model-predicted data. Data not recorded because of local logistical problems are identified by white dots or lines.

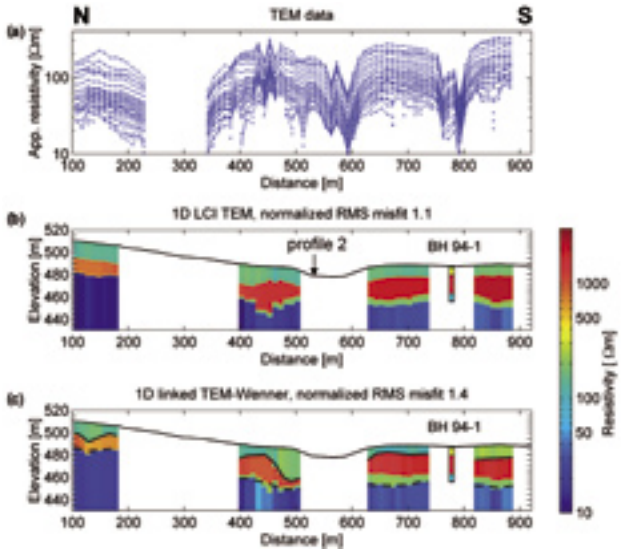

FIGURE 8

(a) TEM data acquired at 10 m spacing along geophysical profile 1. Data points at each station are marked by crosses. Crosses representing common time-gates are connected by solid lines. (b) 1D laterally constrained model of the TEM data. Regions affected by metallic pipes and borehole casing are blanked. (d) 1D linked model of the TEM and Wenner data. Solid and dashed black lines below the surface outline the picked upper and lower edges of the highly resistive zone, respectively. Lithologies in borehole 94-1 are described in Fig. 2.

turning off the transmitter current, the decay of the induced secondary field was recorded between 6.8 and 2792 μs. The data were integrated over an 8 s time-window and six measurements were made at each station to improve signal quality and allow data uncertainty to be estimated. The SiTem software package (HydroGeophysics Group, University of Aarhus, Denmark) was used to process the data. After eliminating noisy or unreliable data, the individual measurements were stacked to form sounding curves at each recording point.

The apparent resistivities in Fig. 8(a) were estimated from the TEM data using a far-field expression (Spies and Frischknecht 1991). During the field campaign, it was obvious that a buried metal pipe would preclude the recording of useful data at distances near 250 m. In addition, Fig. 8(a) demonstrates that data on either side of this distance range and at two other locations were contaminated by the coupling effects of buried pipes and the metal casing of borehole 94-1 (Danielsen *et al*. 2003). To correct for such effects by forward modelling would have required accurate information on the shape and position of the conducting objects and the subsurface layering (Fitterman *et al.* 1990), neither of which were available at the Baltenswil site.

Results of 1D laterally constrained inversion of the TEM data

Inversion of the TEM data is performed using the 1D laterally constrained inversion (LCI) method (Auken and Sørensen 1999; Auken *et al.* 2004; Auken and Christiansen 2004; Auken *et al*. 2005) implemented in the em1dinv software package (HydroGeophysics Group, University of Aarhus, Denmark). This method involves applying a simultaneous 1D inversion scheme to all data not contaminated by the coupling effects of metallic conductors. By minimizing a common objective function, specifying a common number of layers beneath each recording station and constraining nearby 1D models to be similar to each other, the output is a series of 1D models in which the resistivity in each layer varies smoothly from model to model. Since the inversion scheme is based on horizontally layered earth models, it does not account for the effects of surface topography.

In applying the 1D LCI method to the TEM data recorded along profile 1, we set the number of layers to four in anticipation of mapping the boundaries and resistivities of the following four units observed in borehole 94-1: combined topsoil-moraine layer, dry gravel, saturated gravel and weathered Molasse sedimentary rock. The resultant model, shown in Fig. 8(b), has a low normalized RMS misfit of 1.1. We emphasize that the shallowest parts of any earth model are not well constrained by data recorded in the 6.8–2792 μs time range, such that the resistivities in the upper two layers of the model in Fig. 8(b) are poorly resolved; they do not deviate greatly from the input values.

The geometries of the layers in the models of Figs 6 and 8(b) are quite similar, but the lateral and vertical variations of resistivity are noticeably less pronounced in the TEM model than in the geoelectric models. However, a major advantage of the TEM method is its high sensitivity to vertical transitions from high to low resistivities (Raiche *et al*. 1985). Accordingly, the depths to the boundaries of the high-resistivity layer in Fig. 8(b) are well resolved (e.g. compare the model boundaries with those encountered in the borehole).

We emphasize that the thin layer of intermediate resistivities underlying the high-resistivity layer along a large portion of profile 1 (Fig. 8b) was consistent with, but not required by, the TEM data. It was introduced to satisfy the observations of water-saturated gravel within boreholes 94-1, 94-2, 14 and 94-4 (Fig. 2). Equally good fits to the data were obtained by using three-layer models in the inversion process.

Results of 1D linked inversions of the TEM and Wenner data

To combine the relatively high resolution information at shallow depths provided by the geoelectric method with the superior resolution at greater depths supplied by the TEM method, joint or linked inversions of the two types of data are desirable. Such inversions should also reduce the well-known ambiguities associated with inversions of the individual data sets (Vozoff and Jupp 1975; Raiche *et al.* 1985; Sandberg 1993; Maier *et al*. 1995; Auken *et al.* 2001; Christiansen *et al.* 2004). To our knowledge, there are currently no algorithms that allow geoelectric and TEM data, recorded across terrain with varying topographic relief, to be jointly inverted in terms of 2D resistivity models, but the laterally constrained inversion approach is capable of providing

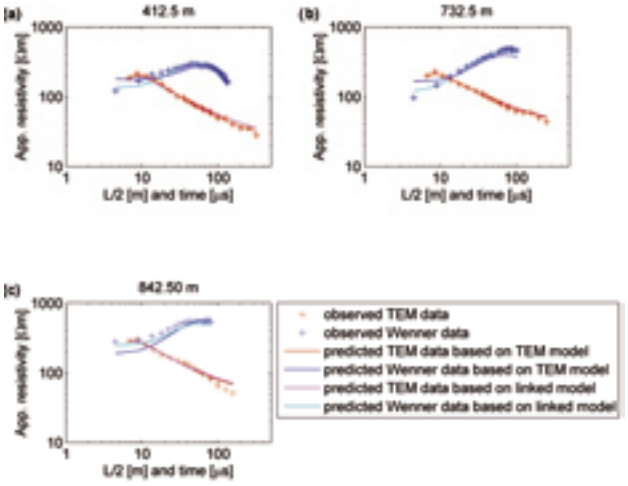

FIGURE 9

Ccomparison of observed Wenner and TEM data with simulated data, based on the individual and linked TEM models, for three typical sounding points.

linked suites of 1D geoelectric and TEM models. This is achieved by including similarity information between neighbouring geoelectric and TEM data and transferring information between converging geoelectric and TEM models during the simultaneous inversion process (Auken *et al.* 2001; Christiansen *et al.* 2004; Sørensen *et al*. 2005). A number of laterally constrained inversions were performed by linking the individual and combined geoelectric data sets (Fig. 5) with the TEM data (Fig. 8a). The best results were obtained with the Wenner data (Fig. 5a), primarily because they had the highest signal-to-noise ratios and were least affected by the buried metal pipes and metal casing of borehole 94-1 (e.g. note the normalized RMS misfit of only 0.6 in Fig. 6a).

The 1D linked TEM-Wenner models in Fig. 8(c) have a moderately low normalized RMS misfit of 1.4. A comparison of responses predicted by the TEM and linked TEM-Wenner models with the observed data at three typical locations, is shown in Fig. 9. In all examples, the 1D LCI TEM models predict values that match closely the observed TEM data and are in the same general range as the Wenner data. Nevertheless, predicted Wenner values in Fig. 9(a,b) are too high at short turn-off times and too low at most turn-off times in Fig. 9(c). In contrast, the linked TEM-Wenner models predict values that are close to all Wenner data at all turn-off times, while maintaining good matches to all TEM data.

Although layer geometries in the TEM and linked TEM-Wenner models in Fig. 8(b,c) are quite similar, the lateral resistivity variations appear to be more plausible in the linked models. They follow the same general trends in the upper two layers as seen in the 2D geoelectric models of Fig. 6; in particular, note the distinct north to south increase in resistivity of the second layer.

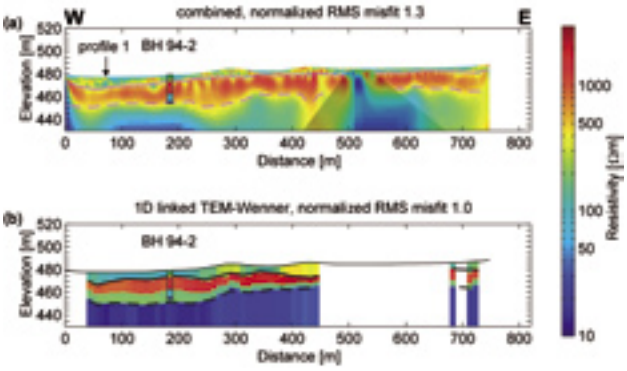

FIGURE 10

(a) 2D resistivity model for profile 2 obtained by inverting the combined Wenner, Schlumberger and dipole–dipole data sets. The same electrode configurations were used as for profile 1. The region contaminated by the 3D effects of a buried pipe is covered by a transparent screen. (b) 1D linked model of the TEM and Wenner data. Lithologies in borehole 94-2 are described in Fig. 2. The 1.3 nomalized RMS misfit for the inversion of the combined geoelectric data set corresponds to a conventional RMS misfit of 9.6%.

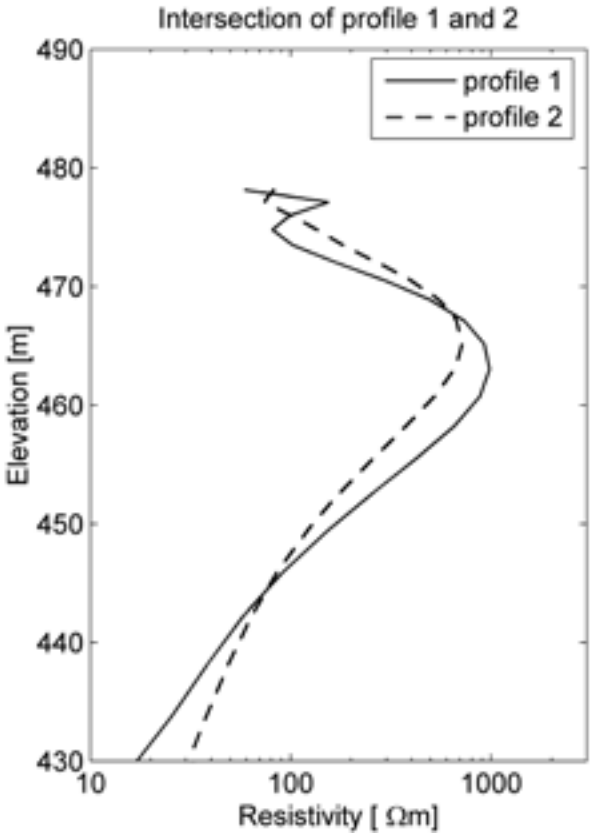

FIGURE 11

Comparison of resistivity values versus depth extracted from the 2D resistivity models for geophysical profiles 1 and 2 at their common intersection point.

2D geoelectric and transient electromagnetic surveys: results from profile 2

Since the seismic data collected along profile 1 provided no useful information on the target gravel layer (reflection seismic processing was not successful in revealing the presence of appropriately shallow features), for profile 2 we focused our efforts on the geoelectric and TEM methods using the same acquisition parameters as employed for profile 1. Models obtained from the 2D tomographic inversion of the combined geoelectric data and the 1D linked inversion of the TEM and Wenner data are shown in Fig. 10. The two models are structurally similar, with both containing a high-resistivity layer associated with the gravel layer. As for profile 1, the overlying loamy topsoil and morainal layers have intermediate resistivities and the underlying weathered Molasse sedimentary rock has low resistivities.

In Fig. 11, we compare resistivity–depth profiles extracted from the 2D resistivity tomograms of Figs 6(d) and 10(a) at their common intersection point. Considering that the geoelectric data are independent along the two profiles and no attempt is made to force similarity in the vicinity of the intersection, the correspondence between the two resistivity–depth profiles is very good.

INTEGRATED INTERPRETATION

In an attempt to combine subsurface information from the various sources at the Baltenswil investigation site, we plot in Fig. 12(a,b): (i) the interface between the loamy topsoil and underlying morainal material based on the tomographic inversion of seismic first-arrival traveltimes (solid blue line); (ii) the boundaries of the gravel layer as determined from the 2D tomographic inversions of the geoelectric data (dashed and solid red lines) and the 1D linked inversions of the TEM and Wenner data (dashed and solid green lines); (iii) the groundwater table that is consistent with the 1D linked inversions of the TEM and Wenner data (dashed blue lines); and (iv) lithological details from the two boreholes. Based on this combined information, we present in Fig. 12(c,d) our best estimates of the subsurface lithologies beneath the two geophysical profiles.

The abrupt vertical P-wave velocity increase in the seismic tomogram allows the base of the loamy topsoil to be delineated along the length of the seismic profile (Fig. 12a). It is noteworthy that this interface is not delineated in any of the electrical resistivity models (Figs 6 and 8). In contrast, the upper and lower boundaries of the high-resistivity gravel layer are quite well defined in the 2D resistivity and 1D linked TEM-Wenner models. Where the depth estimates to the upper boundary differ significantly in the two suites of models, we choose the values provided by the 2D resistivity model; geoelectric methods are much more sensitive to resistivity variations in the shallow subsurface than TEM methods and the influence of surface topography is included in inversions of the geoelectric data. By comparison, at the one location where the depth estimates to the lower boundary differ significantly

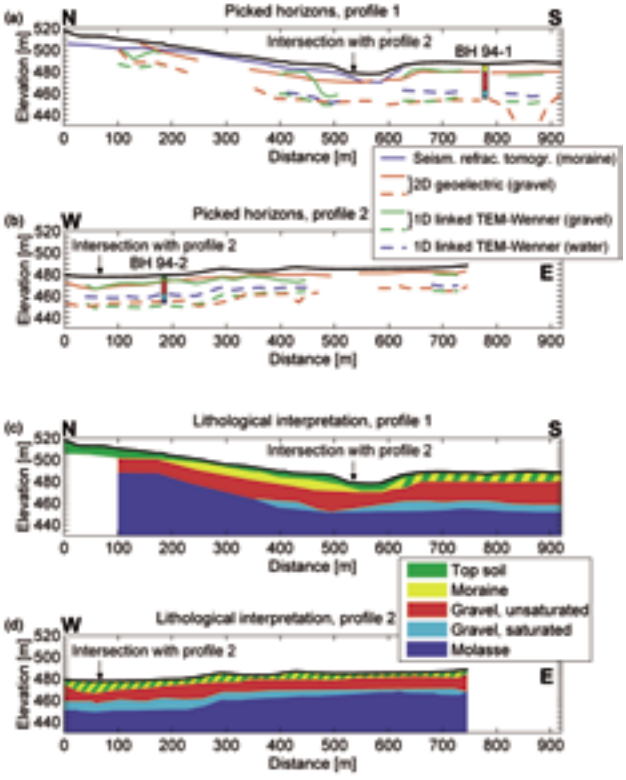

FIGURE 12
Comparison of the picked horizons based on the tomographic seismic refraction model, 2D resistivity models and 1D linked TEM-Wenner models for (a) profile 1 and (b) profile 2. Lithologies in boreholes 94-1 and 94-2 are described in Fig. 2. Interpreted lithologies based on an integrated interpretation of all borehole and geophysical data for (c) profile 1 and (d) profile 2.

in the two suites of models (i.e. at 800 to 900 m distance along profile 1), we choose the values supplied by the 1D linked TEM-Wenner models; TEM methods are more sensitive to deep resistivity variations and, in particular, to vertical changes from high to low resistivity (Raiche *et al.* 1985). If our choice is correct, then the anomalous thickening of the high-resistivity layer at 800–900 m in the geoelectric models of profile 1 is an artefact.

A boundary between unsaturated and saturated gravels (i.e. the groundwater table) is not essential to explain any of our geophysical data sets. However, the relatively low resistivities of the groundwater and the high porosities of gravel demand that there be a decrease in resistivity at the groundwater table. If we impose this constraint on the 1D linked inversions of the TEM and Wenner data, then the aquifer would only have a finite thickness below the southern part of profile 1 and beneath profile 2 (Fig. 12c,d). It would be insignificantly thin along the northern part of profile 1 (Fig. 8c), consistent with the absence of water-saturated gravel in borehole 94-3.

TABLE 1
Strengths and weaknesses of geophysical methods as applied at the Baltenswil site

Method	Strengths of geophysical methods as applied at Baltenswil	Weaknesses of geophysical methods as applied at Baltenswil
2D seismic refraction with inversion based on L_2-norm	• Provides relatively high-resolution information on the shallow subsurface • Surface topography is included in the inversions	• Requires good ground contact • Large effort for data acquisition and analysis • Limited depth penetration in regions characterized by high vertical velocity gradients • Images are somewhat blurred • Depending on the presence or not of low velocity and/or thin high-velocity layers, there may be ambiguities in the inversions
2D geoelectric with inversion based on L_2-norm	• Efficient data acquisition and analysis • Negative effects of buried metal objects extend over relatively small areas • Surface topography is included in the inversions • Cost effective	• Requires good ground contact • Poor resolution beneath highly resistive layers • Images are somewhat blurred • Ambiguities in the inversions
1D TEM with laterally constrained inversion	• Efficient data acquisition and analysis • Requires no direct ground contact • Large penetration depth • Cost effective	• Variations in surface topography may cause artefacts in the derived models • Negative effects of buried metal objects extend over wide areas • Ability to resolve the very shallow subsurface is limited • Ability to determine the exact resistivity of highly resistive structures is low • Ambiguities in the inversions
1D TEM and geoelectric with linked laterally constrained inversion	• Efficient data acquisition and analysis • Large penetration depth • Model ambiguity reduced relative to inversions of single data types • Cost effective	• Variations in surface topography may cause artefacts in the derived models • Negative effects of buried metal objects extend over wide areas • Although reduced relative to single-technique approaches, ambiguities persist in the inversions

STRENGTHS AND WEAKNESSES OF GEOPHYSICAL METHODS AS APPLIED AT BALTENSWIL

In Table 1, we summarize the strengths and weaknesses of geophysical techniques as employed in our investigation of the Baltenswil catchment. The tomographic seismic refraction technique supplied useful information on the shallow subsurface, but only after significant effort was put into acquiring and processing large volumes of data. Moreover, the high vertical velocity gradient at shallow depths limited the depth penetration of the first-arriving energy. Even though traveltimes were picked to ~100 m distance, the first arrivals travelled no deeper than 10–20 m (Fig. 4), such that the target gravel layer was not illuminated. To overcome this depth limitation, the seismic energy would need to be transmitted over longer distances. Since aquifer protection policies prohibit the use of explosives and other high-energy sources at the Baltenswil site, this option is currently not feasible.

Acquisition and processing of the geoelectric and TEM data were relatively speedy processes. During an eight-hour day, it was possible for a two-person crew either to record 10 000 apparent-resistivity values using the GeoTom 100-electrode

acquisition system or to make 40 TEM soundings using the ProTEM 47D system. However, metal objects above and below the ground reduced the applicability of both methods at several locations. In addition, in our interpretations of the resistivity models, it was necessary to take into account ambiguities associated with inversions of the data. By combining information contained in the geoelectric and electromagnetic data, it was possible to broaden the depth range of investigation and reduce the interpretational non-uniqueness (Table 1).

CONCLUSIONS

We have acquired, processed and interpreted frequency-domain electromagnetic, tomographic seismic refraction, transient electromagnetic and geoelectric data across a small but important well catchment in northern Switzerland. The primary objectives were to determine the geometries and physical properties of the shallow sedimentary layers and map the depth to the groundwater table. Data acquisition, processing and inversion of the various data sets were complicated by natural and anthropogenic features (e.g. topographic relief, buried metal pipes and other metal objects, insufficient boreholes). Nevertheless, the interface between the surface loamy topsoil and underlying morainal material was well defined in the P-wave velocity model, and the upper and lower boundaries of the important water-bearing gravel layer were delineated in resistivity models derived from the geoelectric and transient electromagnetic data.

ACKNOWLEDGEMENTS

We thank Dr. M.H. Loke for extending his geoelectric inversion routine to include large data sets and for improving the topography component of the method, Professor W. Kinzelbach for his suggestion to investigate the Baltenswil site, Dr. A.V. Christiansen, Mr. N. Foged and Mr. G.A. Onnis for their involvement in the project, and the journal reviewers and editors for their constructive comments. This research was supported by the Swiss National Science Foundation.

REFERENCES

Amt für Abfall, Wasser, Energie und Luft Kanton Zurich, 1998. *Grundwasserpumpwerk Baltenswil, Nitrat-Pilotprojekt: Ergebnisse der hydrogeologischen Untersuchungen 1994-1997 (Groundwater pumping station Baltenswil, Nitrate pilot project: results of the 1994-1997 hydrogeological investigation)*. Report submitted by Dr. Jäckly AG to the Amt für Abfall, Wasser, Energie und Luft Kanton Zurich, Abteilung Wasserwirtschaft, Baudirektion Zurich.

Auken E. and Christiansen A.V. 2004. Layered and laterally constrained 2D inversion of resistivity data. *Geophysics* **69**, 752–761.

Auken E., Christiansen A.V., Jacobsen B.H., Foged N. and Sørensen K.I. 2005. Piecewise 1D laterally constrained inversion of resistivity data. *Geophysical Prospecting* **53**, 497–506.

Auken E., Christiansen A.V., Jacobsen L. and Sørensen K.I. 2004. Laterally constrained 1D-inversion of 3D TEM data. 10th European Meeting on Environmental and Engineering Geophysics, EAGE Near Surface, Expanded Abstracts, A008.

Auken E., Pellerin L. and Sørensen K. I. 2001. Mutually constrained inversion (MCI) of electrical and electromagnetic data. 71st SEG Meeting, San Antonio, Texas, USA, Expanded Abstracts, 1455–1458.

Auken E. and Sørensen K.I. 1999. Laterally constrained inversion of densely measured profile oriented EM data in "soft" 3D sedimentary environments. 69th SEG Meeting, Houston, USA, Expanded Abstracts, 232–236.

Christiansen A.V., Foged N., Auken E. and Srensen K.I. 2004. Integrated Inversion of CVES and TEM data using lateral constraints. 10th European Meeting on Environmental and Engineering Geophysics, EAGE Near Surface, Expanded Abstracts, A033.

Dahlin T. 2001. The development of DC resistivity imaging techniques. *Computers and Geosciences* **27**, 1019–1029.

Dahlin T. and Zhou B. 2004. A numerical comparison of 2D resistivity imaging with ten electrode arrays. *Geophysical Prospecting* **52**, 379–398.

Danielsen J.E., Auken E., Jørgensen F., Søndergaard V. and Sørensen K.I. 2003. The application of the transient electromagnetic method in hydrogeophysical surveys. *Journal of Applied Geophysics* **53**, 181–198.

Edet A.E. and Okereke C.S. 2002. Delineation of shallow groundwater aquifers in the coastal plain sands of Calabar area (Southern Nigeria) using surface resistivity and hydrogeological data. *Journal of African Earth Sciences* **35**, 433–443.

Fertig J. 1997. Geschwindigkeits- und Dichtewerte in Sedimenten. In: *Handbuch zur Erkundung des Untergrundes von Deponien und Altlasten Bd.* 3 *Geophysik* (*Handbook for Investigating the Subsurface in the Neighbourhood of Active and Abandoned Landfills, Vol.* 3*, Geophysics*) (eds K. Knödel, H. Krummel and G. Lange), pp. 442–443. Springer, Berlin.

Fitterman D.V., Frischknecht F.C., Mazzella A.T. and Anderson W.L. 1990. Example of transient electromagnetic soundings in the presence of oil field pipes. In: *Geotechnical and Environmental Geophysics, Vol* 2 (ed. S.H. Ward), pp. 79–88. Society of Exploration Geophysicists, Tulsa, Oklahoma.

Fitterman D.V. and Stewart M.T. 1986. Transient electromagnetic sounding for groundwater. *Geophysics* **51**, 995–1005.

Gabriel G., Kirsch R., Siemon B. and Wiederhold H. 2003. Geophysical investigation of buried Pleistocene subglacial valleys in Northern Germany. *Journal of Applied Geophysics* **53**, 159–180.

Goldman M. and Neubauer F.M. 1994. Groundwater exploration using integrated geophysical techniques. *Surveys in Geophysics* **15**, 331–361.

Jørgensen F., Lykke-Andersen H., Sandersen P.B.E., Auken E. and Nørmark E. 2003. Geophysical investigations of buried Quaternary valleys in Denmark: an integrated application of transient electromagnetic soundings, reflection seismic surveys and exploratory drillings. *Journal of Applied Geophysics* **53**, 215–228.

Lanz E., Maurer H.R. and Green A.G. 1998. Refraction tomography over a buried waste disposal site. *Geophysics* **63**, 1414–1433.

Loke M.H. 2000. Topographic modelling in resistivity imaging inversion. 62nd EAGE Conference, Glasgow, Scotland, Expanded Abstracts, D0002.

Loke M.H. and Barker R.D. 1996. Rapid least-squares inversion of apparent resistivity pseudosections using a quasi-Newton method. *Geophysical Prospecting* **44**, 131–152.

Maier D., Maurer H.R. and Green A.G. 1995. Joint inversion of related data sets: DC resistivity and transient electromagnetic soundings. 1st European Meeting on Environmental and Engineering Geophysics, EAGE Near Surface, Expanded Abstracts, 461–464.

McNeill J.D. 1980. *Electromagnetic terrain conductivity measurement at low induction numbers*. Technical Note, **TN-6**. Geonics Ltd, Toronto.

Onnis G.A., Althaus R., Klump S., Hendricks Franssen H.J., Stauffer F. and Kinzelbach W. 2005. Simulating environmental tracer transport in unsaturated-saturated porous media. ModelCARE Conference, The Hague, The Netherlands, Expanded Abstract.

Onnis G.A., Hendricks Franssen H.J., Stauffer F. and Kinzelbach W. 2004. Stochastic inverse modeling of groundwater flow and environmental tracer transport: Baltenswil case study (Switzerland). GeoENV Conference. Neuchâtel, Switzerland, Expanded Abstract.

Osella A., Favetto A., Martinelli P. and Cernadas D. 1999. Electrical imaging of an alluvial aquifer at the Antinaco-Los Colorados tectonic valley in the Sierras Pampeanas, Argentina. *Journal of Applied Geophysics* **41**, 359–368.

Palacky G.J. and Stephens L.E. 1990. Mapping of Quaternary sediments in northeastern Ontario using ground electromagnetic methods. *Geophysics* **55**, 1596–1604.

Raiche A.P., Jupp D.L.B., Rutter H. and Vozoff K. 1985. The joint use of coincident loop transient electromagnetic and Schlumberger sounding to resolve layered structures. *Geophysics* **50**, 1618–1627.

Rubin Y. 2003. *Applied Stochastic Hydrology*. Oxford University Press, Oxford.

Rubin Y. and Hubbard S. (eds) 2005. *Hydrogeophysics*. Springer, New York.

Rubin Y., Mavko G. and Harris J. 1992. Mapping permeability in heterogeneous aquifers using hydrologic and seismic data. *Water Resources Research* **28**, 1809–1816.

Sandberg S.K. 1993. Examples of resolution improvement in geoelectrical soundings applied to groundwater investigations. *Geophysical Prospecting* **41**, 207–227.

Shtivelman V. and Goldman M. 2000. Integration of shallow reflection seismics and time domain electromagnetics for detailed study of the coastal aquifer in the Nitzanim area of Israel. *Journal of Applied Geophysics* **44**, 197–205.

Sørensen K.I., Auken E., Christensen N.B. and Pellerin L. 2005. An integrated approach for hydrogeophysical investigations: new technologies and a case history. In: *Near Surface Geophysics Vol II: Applications and Case histories* (ed. D.K. Butler), pp. 585–606. Society of Exploration Geophysicists, Tulsa, Oklahoma.

Spies B.R. and Frischknecht F.C. 1991. Electromagnetic sounding. In: *Electromagnetic Methods in Applied Geophysics, Vol. 2* (ed. M.N. Nabighian), pp. 285–426. Society of Exploration Geophysicists. Tulsa, Oklahoma.

Stummer P., Maurer H. and Green A.G. 2004. Experimental design: Electrical resistivity data sets that provide optimum subsurface information. *Geophysics* **69**, 120–139.

Vozoff K. and Jupp D.L.B. 1975. Joint inversion of geophysical data. *Geophysical Journal of the Royal Astronomical Society* **44**, 977–911.

Young M.E., de Bruijn R.G.M. and bin Salim Al-Ismaily A. 1997. Exploration of an alluvial aquifer in Oman by time-domain electromagnetic sounding. *Hydrogeology Journal* **6**, 383–393.